THE JOURNAL OF PHYSICAL CHEMISTRY C



pubs.acs.org/JPCC Article

Control of Excited-State Proton-Coupled Electron Transfer by Ultrafast Pump-Push-Probe Spectroscopy in Heptazine-Phenol Complexes: Implications for Photochemical Water Oxidation

Kathryn L. Corp, Emily J. Rabe, Xiang Huang, Johannes Ehrmaier, Mitchell E. Kaiser, Andrzej L. Sobolewski, Wolfgang Domcke, and Cody W. Schlenker*



Cite This: J. Phys. Chem. C 2020, 124, 9151-9160



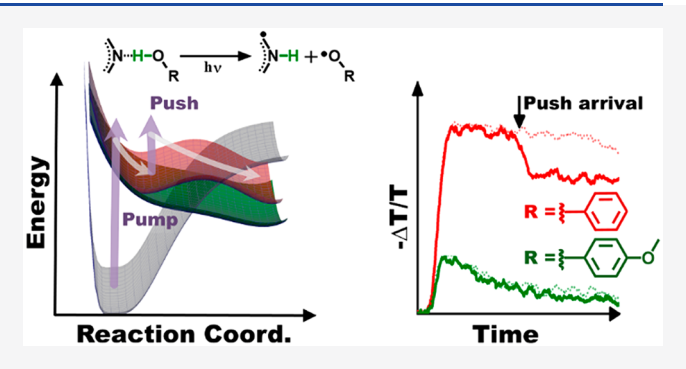
ACCESS

Metrics & More

Article Recommendations

Supporting Information

ABSTRACT: We demonstrate chemical tuning and laser-driven control of intermolecular H atom abstraction from protic solvent molecules. Using multipulse ultrafast pump-push-probe transient absorption (TA) spectroscopy, we monitor hydrogen abstraction by a functionalized heptazine (Hz) from substituted phenols in condensed-phase hydrogen-bonded complexes. Hz is the monomer unit of the ubiquitous organic polymeric photocatalyst graphitic carbon nitride (g-C₃N₄). Previously, we reported that the Hz derivative 2,5,8-tris(4-methoxyphenyl)-1,3,5,6,7,9,9b-heptaazaphenalene (TAHz) can photochemically abstract H atoms from water, in addition to exhibiting photocatalytic activity for H_2 evolution matching that of g-C₃N₄ in aqueous suspensions. In the present



work, we combine ultrafast multipulse TA spectroscopy with predictive wave function-based ab initio electronic-structure calculations to explore the role of mixed $n\pi^*/n\pi^*$ upper excited states in directing H atom abstraction from hydroxylic compounds. We use an ultraviolet (365 nm) laser pulse to photoexcite TAHz to a bright upper excited state, and, after a relaxation period of roughly 6 ps, we use a near-infrared (NIR) (1150 nm) pulse to "push" the chromophore from the long-lived S_1 state to a higher-lying excited state. When phenol is present, the NIR push induces a persistent decrease ($\Delta\Delta$ OD) in the S_1 TA signal magnitude, indicating an impulsively driven change in photochemical branching ratios. In the presence of substituted phenols with electron-donating moieties, the magnitude of $\Delta\Delta$ OD diminishes markedly due to the increased excited-state reactivity of these complexes that accompanies the cathodic shift in phenol oxidation potential. In the latter case, H atom abstraction proceeds unaided by additional energy from the push pulse. These results reveal new insight into branching mechanisms among unreactive locally excited states and reactive intermolecular charge-transfer states. They also suggest molecular design strategies for functionalizing azaromatics to drive important photoreactions, such as H atom abstraction from water. More generally, this study demonstrates an avidly desired achievement in the field of photochemistry, rationally redirecting excited-state reactivity with light.

■ INTRODUCTION

Photochemical reactions occur on time scales of milliseconds to minutes. However, reaction yields are controlled by branching among photophysical pathways occurring on much faster time scales (femtoseconds to nanoseconds). Unfortunately, it is not generally well-understood how these time scales are interrelated. Competition among decay processes such as fluorescence, phosphorescence, internal conversion, intersystem crossing, charge transfer, and H atom tunneling ultimately determine the overall reaction efficiency. Understanding how to manipulate the branching ratios among these excited-state relaxation pathways is likely the key to directing reactivity in photochemical transformations such as CO₂ reduction, water remediation, ^{2,3} acid/base photochemistry, ^{4,5} and artificial photosynthesis. ⁶

Photochemical reactions of aza-aromatics are a compelling testbed for studying light-driven chemistry. Many aza-

aromatics engage in addition, reduction, and substitution reactions when they absorb light in the presence of an appropriate H atom donor.^{7–11} However, the mechanisms of these reactions have been heavily debated in the literature for decades, particularly with regard to how intermolecular hydrogen bonding with H atom donors can control the reactivity of these molecules, ^{12–14} with little clear consensus.

Historically, the rich photochemistry of these *N*-heteroaromatics, such as acridines, purines, and quinolines, in protic

Received: January 15, 2020 Revised: February 21, 2020 Published: March 2, 2020





media was assumed to proceed directly from low-lying locally excited states of the heteroaromatic molecule. 7,11,15 By locally excited states, here we mean those involving only the orbitals of the chromophore, with no contribution from neighboring solvent molecules. Remarkably, until recently, even the electronic configuration of the reactive excited state of acridine, a model nitrogenous heteroaromatic whose photochemistry has been extensively studied for over 70 years, 15-20 continued to be a contentious issue in the literature. In 2014, Eisenhart and Dempsey showed a proton-coupled electron transfer (PCET) mechanism by which the lowest locally excited triplet state drives H atom transfer from phenol (PhOH) to acridine orange.²¹ Using computational methods, Domcke, Sobolewski, and co-workers demonstrated that the H atom abstraction reaction with acridine involves a manifold of charge-transfer (CT) states with electronic configurations comprising both aza-aromatic and hydroxylic orbitals of the H-bonded intermolecular complex.²²

More recently, Domcke, Sobolewski, and co-workers predicted that triazine- and heptazine-based molecules and materials engage in photochemistry analogous to that of acridine. ^{23,24} Heptazine-based materials, such as carbon nitride, have garnered intense interest for photocatalytic hydrogen evolution and water splitting in recent years. ^{3,25–32} While the synthesis of these earth-abundant materials is straightforward, the chemical composition and the molecular structures are ambiguous; therefore, the underlying photophysical and photochemical processes of these catalysts are typically harrowing to control and remain poorly understood. ^{33–37}

To clarify the fundamental photophysics of heptazine-based materials, we recently synthesized the anisole-substituted heptazine (Hz) derivative 2,5,8-tris(4-methoxyphenyl)-1,3,4,6,7,9,9b-heptaazaphenalene (TAHz) (Figure 1a).³⁸

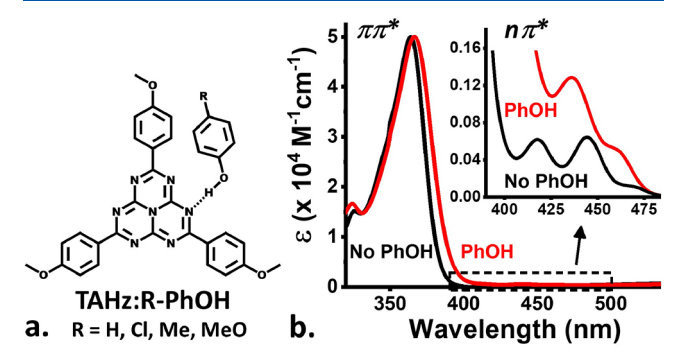


Figure 1. (a) Molecular structure and (b) ground-state absorption spectrum of 2,5,8-tris(4-methoxyphenyl)-1,3,4,6,7,9,9b-heptaazaphenalene (TAHz) in toluene with and without phenol (PhOH) (100 mM).

Using TAHz as a model system, we previously demonstrated that fluorescence from the hydrogen-bonded complex of TAHz with water molecules can be spectroscopically observed and that the complex photochemically reacts to liberate hydroxyl radicals.³⁸ Upon the basis of the excited-state reduction potential of TAHz, the single-electron water oxidation to hydroxyl radicals would not, at first glance, appear to be an accessible process (+2.7 V vs SHE). However, ab initio computational results reveal that the coupling of proton and electron motion can provide a pathway along the H atom transfer coordinate.³⁸ Evidently, the H-bonding interaction modulates the energy of the reacting species via orbital mixing

and the fluctuation of the proton's position along the H-bonding axis.

While photoinduced PCET between Hz-based materials and protic solvent molecules holds potential implications for future energy conversion and storage systems, the carbon nitride literature has focused almost exclusively on proton-reduction reactions to form H₂.^{25–28,39,40} However, as stated above, there is limited knowledge of the underlying photochemical dynamics that control reactions such as H atom abstraction.^{24,41,42} Therefore, it is compelling to examine how local versus intermolecular electronic excitations can provide control over photochemical reaction pathways, such as a single-electron oxidation of hydroxylic compounds.

In this Article, we use ultrafast pump-push-probe spectroscopy in combination with accurate ab initio electronicstructure calculations to control and understand the excitedstate branching ratios of TAHz in the presence of four PhOH derivatives. We employ a series of substituted PhOHs, R-PhOH, to induce a change in photochemistry that would be analogous to that of installing electron-withdrawing groups on the Hz core. We chose this system based on two criteria: (1) the improved solubility of TAHz in toluene vs water and (2) the ease with which we can tune the energy of the intermolecular charge-transfer (CT) state by varying the electron-donating/withdrawing character on the proton source (i.e., R-PhOH). Using ultrafast pump-push-probe spectroscopy, we are able to manipulate the population of the lowestenergy locally excited state by selectively pushing it into higher-lying intermolecular CT states. We show that the relative decrease of the induced absorption ($\Delta\Delta$ OD) from the hydrogen-bonded complex upon the arrival of the push pulse exhibits an anticorrelation with the photochemical reactivity of TAHz:R-PhOH. That is, the effect of the push pulse decreases as the driving force for electron/proton transfer increases. These results, combined with the results of ab initio calculations, provide insight into the ability of short-lived excited states to drive fundamental photochemical reactions. From this knowledge, we can develop design rules for selectively promoting a variety of photochemical reactions with protic solvent molecules.

■ RESULTS AND DISCUSSION

For TAHz:R-PhOH complexes, we previously explored trends in properties such as kinetic isotope effects using fluorescence quenching. While that study revealed new insight into the reactivity of the lowest excited electronic state (S_1) of the complex, it provided no handle for studying the dynamics of the bright upper excited state that may strongly influence photochemistry. The role of upper excited states in driving the photoexcited complex along reactive trajectories remains unclear. Herein, we report the application of ultrafast multipulse TA spectroscopy of these TAHz complexes to correlate their response to an additional "push" pulse with their photochemical reactivity.

In Figure 1a, we present the structure of TAHz hydrogen-bonded to R-PhOH. The absorption spectrum of TAHz in toluene exhibits a redshift in the $\pi\pi^*$ absorption as well as a blueshift of the nearly dark $n\pi^*$ transitions in the presence of PhOH, as shown in Figure 1b. This shift results from the ground-state H-bonding interaction indicated by a dotted line in Figure 1a. Because of the concomitant redshift of the $\pi\pi^*$ energy and blueshift of the $n\pi^*$ energy, these transitions become increasingly mixed upon H-bonding. Therefore, we

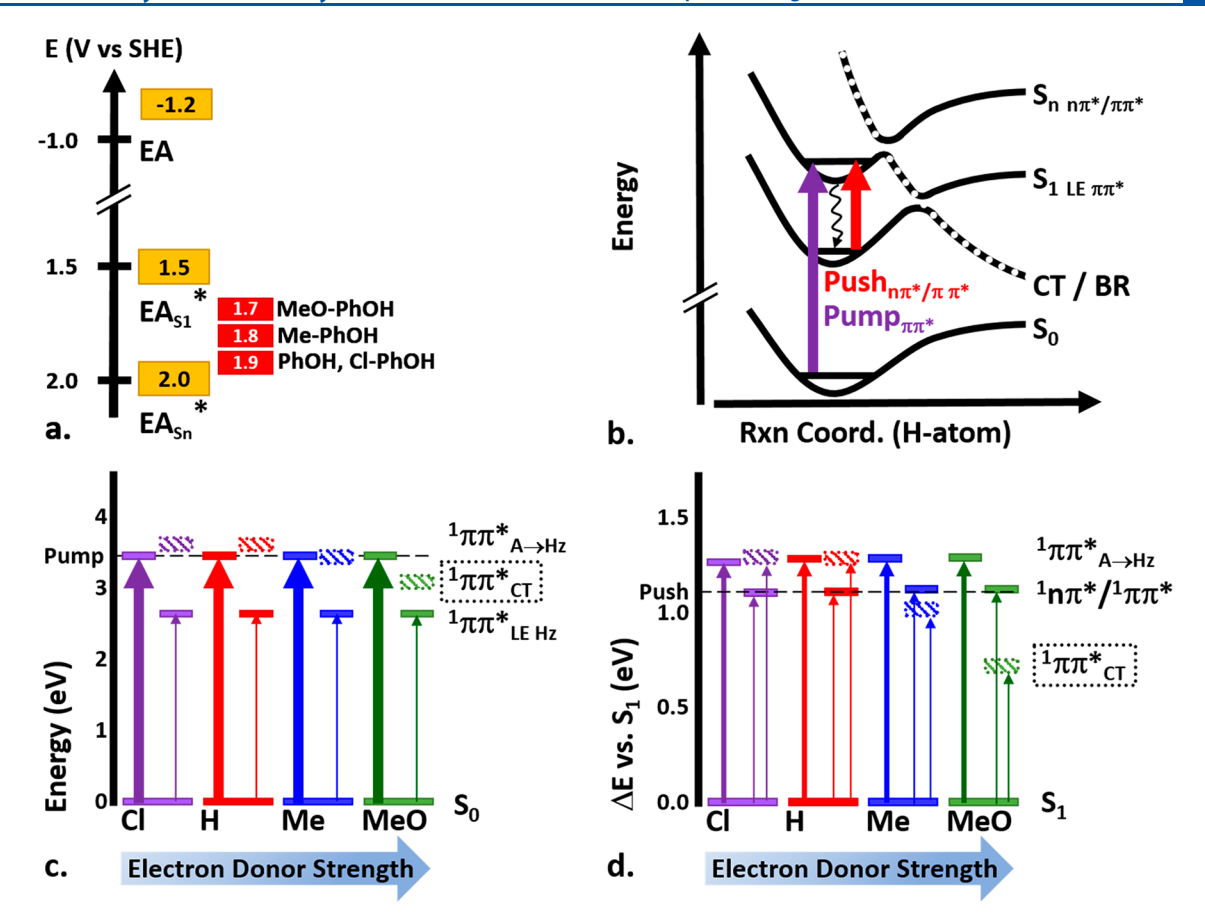


Figure 2. (a) Approximate excitation energies of the excited states of TAHz and oxidation potentials of four phenol derivatives, R-PhOH. As the PhOH oxidation potential shifts cathodically, the thermodynamics for charge transfer after a Hz-localized excitation becomes more favorable. (b) Potential energy diagram showing a photochemical proton-transfer reaction driven by an electronic charge-transfer (CT) state, which is strongly stabilized by the proton transfer, resulting in the formation of a biradical (BR). The push pulse populates higher excited states that can efficiently couple to the CT state. The wavy line indicates rapid radiationless decay of the S_n states to the long-lived S_1 state. (c) Simplified diagram depicting the vertical excitation energies from the electronic ground state to the locally excited dark (LE Hz) and bright ($A \rightarrow Hz$) $^1\pi\pi^*$ states and the intermolecular charge-transfer (CT) state. While the energies of the locally excited states are independent of the substituent R on phenol, the energy of the CT state is substantially lowered by electron-donating substituents such as Me or MeO. (d) Simplified diagram depicting electronic transition energies from the relaxed geometry of the S_1 state. Calculated oscillator strengths for transitions in (c) and (d) are qualitatively represented by the line widths of the vertical arrows. A full quantitative list of transition energies, oscillator strengths, and dipole moments associated with (c) and (d) are reported in the Supporting Information, Tables S1 and S2. Pump and push energies are represented by the black horizontal dashed lines in (c) and (d). Note the different ordinate scales in (c) and (d).

refer to the high-lying state as mixed $n\pi^*/\pi\pi^*$, whereas the lowest-lying state, S_1 , is a pure $\pi\pi^*$ state that is dark in absorption/emission from/to S_0 , respectively.

The approximate oxidation potentials of the R-PhOH in this study are shown in Figure 2a. 45-48 Increasing the strength of the electron-donating substituent on R-PhOH shifts the oxidation potential cathodically.

To glean more insight into the relative energies of excited states of the H-bonded TAHz:R-PhOH complexes, we turned to ab initio quantum chemical calculations. We employed the second-order algebraic-diagrammatic-construction (ADC(2)) method. DC(2) is a wave function-based single-reference propagator method that provides an accurate and balanced description of locally excited states and CT states, which is essential for determining reliable vertical excitation energies of the electronic states involved in excited-state PCET reactions. Figure 2c summarizes the relevant vertical transition energies ($\Delta E/eV$) and oscillator strengths (f) associated with optical transitions from the electronic ground state (S_0). Oscillator strengths are represented qualitatively by the line width of the

vertical arrows, while state energies relative to S_0 are represented by the colored horizontal bars. A full quantitative list of transition energies, oscillator strengths, and dipole moments associated with (c) and (d) is reported in Tables S1 and S2 of the Supporting Information.

The lowest excited singlet state (S_1) is an essentially dipole-forbidden ${}^1\pi\pi^*$ transition, which is a local excitation (LE) on the Hz core. The lowest bright excited state is an intra-molecular $\pi\pi^*$ excitation in TAHz due to electron transfer from the pendent anisole group, A, to the Hz core. This A \rightarrow Hz intramolecular ${}^1\pi\pi^*$ state is very bright and corresponds to the transition with the greatest oscillator strength in Figure 2c, consistent with the absorption signatures that we observe in our experimental spectra at wavelengths shorter than \sim 400 nm. At intermediate energies, between the S_1 state and the bright intramolecular ${}^1\pi\pi^*$ A \rightarrow Hz CT state, there exist a manifold of dark ${}^1n\pi^*$ states, which, for clarity, have been omitted from Figure 2c and Table S1. As such, hereafter we label the pertinent electronic states that reside vertically above S_1 as S_n or according to their predominant orbital character.

We note that, due to vibronic intensity borrowing, two of the dark state transitions faintly appear in our experimental spectra within the range of 400–475 nm in Figure 1b. Most importantly, there exists a singlet state of intermolecular $\pi\pi^*$ CT character, in which an electron is excited from R-PhOH to TAHz or, equivalently, a hole is transferred to R-PhOH from TAHz. In contrast to the intramolecular $^1\pi\pi^*$ A \rightarrow Hz CT state, the intermolecular $^1\pi\pi^*$ CT state transition is optically dark at the geometry of the S_0 state (no vertical arrow in Figure 2c and $f\approx 0.0$ in Table S1).

Inspection of Figure 2c reveals that the energy of the lowest singlet state (S_1) of the complex as well as the energy of the bright $\pi\pi^*$ state are not affected by the R substituent of the R-PhOH derivative. In sharp contrast, we find a significant range of energies for the intermolecular $^1\pi\pi^*$ CT state. The energy of this CT state depends strongly on the nature of the R group linked to the phenol. The vertical excitation energy of this state, which provides the driving force for the proton transfer from R-PhOH to TAHz, decreases from 3.64 eV for Cl-PhOH to merely 3.09 eV for MeO-PhOH. The stronger electrondonating character of the R group leads to an intermolecular CT state of lower energy.

In the case of the TAHz:PhOH complex, the vertical excitation energy of the intermolecular CT state is higher than the energy of the lowest bright $\pi\pi^*$ state. In the case of MeO-PhOH, on the other hand, the intermolecular CT state is vertically below the lowest bright ${}^{1}\pi\pi^{*}$ state; see Figure 1c. From these computational results, one can anticipate that, when the TAHz:MeO-PhOH complex absorbs a photon from the pump pulse at 365 nm, the system will rapidly (on femtosecond time scales) nonadiabatically convert to the CT state and will be propelled along the proton-transfer coordinate to the biradical (BR) product. On the other hand, for the case of the TAHz:PhOH and TAHz:Cl-PhOH complexes, one anticipates that significantly fewer photoexcitations will result in BR products following illumination at 365 nm because the resulting wave packet on the S_n surface must tunnel through a potential energy barrier along the H atom transfer coordinate or traverse the barrier in an activated process if any photochemistry is to occur prior to the fast radiationless relaxation of the system to the long-lived S_1 state.

On the basis of these computational results, we hypothesize that the reactivity pattern for these hydrogen-bonded TAHz:R-PhOH complexes should generally map onto the schematic potential energy diagram shown in Figure 2b. That is, the energy of the CT/BR state is lowered with increasing electrondonating strength of the substituent on R-PhOH, which should result in an increase in radical products.⁴³ To experimentally probe whether this is true, we employed spin-trapping electron paramagnetic resonance (EPR) spectroscopy to compare the radical yields for TAHz:MeO-PhOH vs TAHz:PhOH as two limiting cases. For these spin-trapping experiments, we utilized 5,5-dimethyl-1-pyrroline N-oxide (DMPO) as a phenoxyl radical scavenger to form metastable radical products with lifetimes long enough to be detected by steady-state EPR. Figures S1a and b of the Supporting Information show that the EPR spectra collected in this work match literature precedent.⁵⁰ In Figure S1c, we show a substantial increase (roughly 40%) in the initial DMPO-phenoxyl radical adduct concentration upon illuminating the TAHz:MeO-PhOH complex at 365 nm compared to illuminating the TAHz:PhOH complex. The higher radical generation yield in the case of MeO-PhOH suggests that changing the excited-state energy

landscape has a large influence on the postexcitation photophysical branching ratios and ultimate photochemical reaction yields in this system.

Having established the character of the ground-state absorption spectra, the excited-state energies, and the general trend in radical yields for our TAHz:R-PhOH complexes, we turn to transient absorption (TA) spectroscopy to probe the upper excited-state dynamics on femtosecond to nanosecond time scales for this chemical series. Figure 3a depicts the

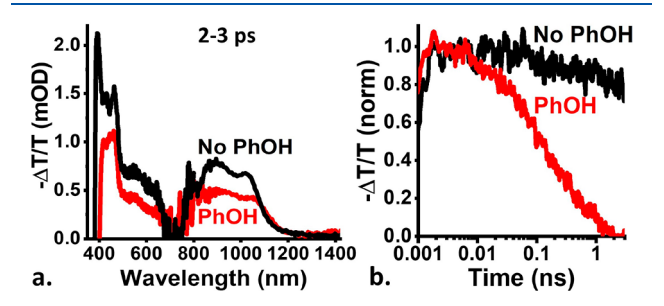


Figure 3. (a) Transient absorption spectra from the ultraviolet to near-infrared (averaged from 2-3 ps) and (b) decay traces of TAHz (15 μ M) with and without phenol (PhOH) (1.0 M) averaged over 900–1000 nm.

transient absorption spectra for toluene solutions of TAHz in the presence and absence of PhOH. In this case, we have employed probe wavelengths ranging from 400 to 1400 nm, integrated over 2–3 ps after the arrival of the 365 nm pump pulse. The majority of the signals in both cases comprise an induced absorption spanning the gamut of the probe wavelengths that we utilized in this study.

To identify the nature of the broad induced absorption features that we observe in Figure 3a, we focus on the NIR portion of the transient absorption spectrum. We compare the lifetime of the luminescence from S_1 and the lifetime of the excited-state absorption in neat toluene (without the presence of an H atom donor) in Figure S2. We see virtually indistinguishable decay kinetics for the photoluminescence and NIR-induced absorption with a monoexponential decay constant of roughly 300 ns. On the basis of these results, we associate the induced absorption signal in Figure 3a with the population of the lowest-lying singlet excited state, S_1 .

Figure 3 also shows static (a) and dynamic (b) quenching of the excited-state absorption of TAHz in the presence of PhOH. This quenching is evidently due to a new relaxation pathway, which leads to ·TAHzH/PhO· biradical species that ultimately produce the phenoxyl radicals that we detected in our initial spin-trapping EPR experiments mentioned earlier. In addition to quenching, the excited-state absorption changes shape slightly. Notable changes include the slight redshift of the bleach in the UV region, which is expected from the ground-state absorption shift seen in Figure 1b, and the slightly more pronounced redshift at low energies, more clearly seen in Figure S3a and b. This shift is due to hydrogen-bonded TAHz as opposed to free TAHz molecules in toluene solution. We note that the lack of signal in the 700-800 nm region is likely a combination of low probe light after filtering out the fundamental beam (800 nm) and scattered second-order pump light (730 nm).

Upon the basis of its kinetic correlation with the fluorescence decay that we observe, the TA signal in Figure 3 is generally attributable to excited-state absorption from the

long-lived $S_1 \pi \pi^*$ state of TAHz, as indicated in Figure 2b. To gain further detailed insight into the phenomena exhibited by our excited-state absorption spectra, we once again turned to ab initio electronic-structure calculations. The relevant parameters for excitation from the first singlet excited state (S_1) are depicted in Figure 2d. The vertical transition energies $(\Delta E^*/\text{eV})$ and oscillator strengths (f^*) are tabulated in Table S2, along with the dipole moment (μ /Debye) and dominant electronic configurations of the excited electronic states. These results were obtained in an analogous fashion to those presented earlier for the absorption from the electronic ground state using the ADC(2) method, but the excitation in this case is taken to occur from the equilibrium geometry of the longlived S₁ excited state. The two lowest transitions when exciting from S_1 are the transition to the lowest $n\pi^*$ state of the heptazine core and the transition to the lowest intramolecular $(A \rightarrow Hz)$ CT state. The energies of these transitions are largely independent of the nature of the R pendent group in R-PhOH. By coincidence, these two transitions happen to be nearly degenerate, and their energies are roughly 1.1 eV (λ = 1130 nm) across the board for each TAHz complex that we analyzed in this study (see Table S2 in the Supporting Information). Upon inspection of our transient absorption spectra for the TAHz:PhOH case in Figure 3a, we find that these calculated transition energies are commensurate with the induced absorption signal near 1050 nm, with intensity out to 1200 nm. In general, the oscillator strengths for the transitions from the S_1 state (f^*) are significantly lower than the groundstate f values. This result appears to be qualitatively consistent with our experimental observations based upon a comparison of the magnitude of the excited-state absorption signal relative to that of the ground-state bleach signature.

Interestingly, at energies just above the intramolecular (A \rightarrow Hz) CT state for the R = H and R = Cl complexes, there is the intermolecular CT state that now exhibits nonzero oscillator strength (see Table S2). This is the same CT state from R-PhOH to TAHz as in Table S1. It stands out by its remarkable dipole moment of 11-25 D. It is also worth noting that the oscillator strength for the excitation from the S₁ state to the intermolecular CT state is of the same order of magnitude as the oscillator strength for the excitation to the A \rightarrow Hz intramolecular CT state from the S₁ state. Our calculations also reveal a manifold of higher-energy A -> Hz intramolecular excited-state absorption features that agree well with our experimental results. For example, the next optically allowed transition that we predict resides at 1.81 eV, which is commensurate with the onset of the TA signal that we observe near 690 nm. Notably, for the case of R = Me and R = MeO, the energy of the photochemically reactive intermolecular CT state drops below the energy of the lowest A \rightarrow Hz intramolecular ${}^{1}\pi\pi^{*}$ state (see Figure 2d).

From these spectroscopic measurements and ab initio predictions, the schematic portrayal in Figure 2 begins to emerge for the TAHz:R-PhOH system. The complex can absorb a photon from our 365 nm pump pulse, which excites the bright $\pi\pi^*$ (A \rightarrow Hz) transition calculated at 3.45 eV (360 nm); see Table S1. In the case of TAHz:PhOH, the vertical excitation energy of the optically dark intermolecular CT state is \sim 0.2 eV higher at the S₀ equilibrium geometry than the energy of the lowest bright state. The bright $\pi\pi^*$ state can mix by nonadiabatic coupling with the reactive intermolecular CT manifold, and population may proceed along the proton-transfer coordinate to biradical (BR) products. This process

competes with fast nonreactive radiationless relaxation to the long-lived S_1 state. From the S_1 state, the potential energy barrier along the proton-transfer coordinate is much larger. In the S_1 state, however, the TAHz unit undergoes an out-of-plane deformation that cranes the central nitrogen atom out of the molecular plane. This puckering of the Hz frame allows the $n\pi^*$ states to mix with the $n\pi^*$ states. As a result, optical transitions from the long-lived S_1 state to the mixed upper S_n $(n\pi^*/n\pi^*)$ states become allowed. To explore this new transition experimentally, we introduce a NIR laser pulse that follows the pump pulse to impart additional energy to the S_1 state, transiently "pushing" the population of the S_1 state to higher energy.

We selected $\lambda = 1150$ nm for our NIR push pulse wavelength, such that it would be slightly on the red edge of the lowest-energy excitation predicted from the S_1 state (1130 nm) and the TA signal that we observe experimentally. This is depicted in Figure 4a. In the presence of PhOH, the decay of

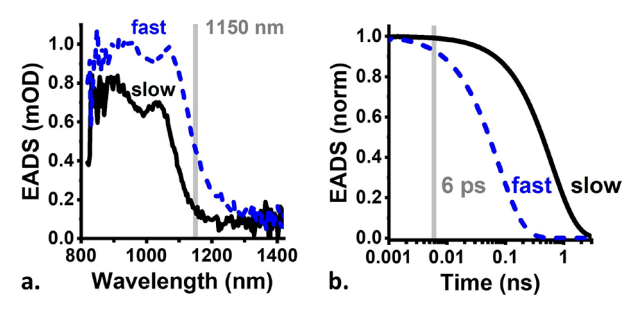


Figure 4. Global analysis (a) spectra and (b) kinetics of the NIR transient absorption feature of TAHz (15 μ M) in the presence of phenol (PhOH) (1.0 M). From the evolution-associated difference spectra (EADS), the push pulse was chosen to be 1150 nm to excite the red edge of the lowest-energy transition for the hydrogen-bonded complex (75 ps decay constant, shown in blue). The long-lived component (shown in black) has a decay constant of 620 ps.

the induced absorption contains a noticeable subnanosecond component (fast), shown in blue, as well as a longer-lived component (slow), shown in black (Figure 4b). We use global analysis to kinetically resolve these features and recover the evolution-associated difference spectra (EADS). We take the overall spectrum, $\psi(t, \lambda)$, to be a linear combination of a timedependent concentration, $c_i(t)$, of the associated species with a wavelength-dependent spectrum, $\sigma_i(\lambda)$, for the *i*th species, such that $\psi(t, \lambda) = \sum c_i(t)\sigma_i(\lambda)$. Figure 4 shows (a) the EADS of the NIR transient absorption spectrum (~800-1400 nm) and (b) their decay traces in the presence of PhOH (1.0 M). We recover two distinct EADS, one with a decay constant of roughly 620 ps and the second with a decay constant of roughly 75 ps. The spectrum of the prompt component is redshifted compared to the longer-lived evolution-associated spectrum. Figure S4 shows the luminescence of TAHz in a similar H-bonded environment that has almost identical evolution-associated decay constants.

We regard the intermolecular CT state as providing the driving force toward \cdot TAHzH/PhO \cdot biradical products, as indicated in Figure 2b. Populating the bright upper excited states, S_n, may provide a pathway to the reactive CT state because the activation barriers are predicted to be low in these upper states. However, these high-lying excited states are relatively short-lived (<200 fs) (see Figure S5), implying that the biradical product yield might intrinsically be low if this

were the only excited-state PCET reactivity pathway. Ideally, for optimum biradical yield, the system should be designed such that there is no energetic barrier from the lowest-lying bright state to the CT state in order to minimize the additional excitation energy needed to drive reactivity.

To uncover the dynamics at the excited-state curve crossings on photochemical H atom transfer reactions between TAHz and PhOH derivatives, we employ a multipulse ultrafast transient absorption technique. A simplified experimental setup and pulse sequence of this technique are found in Figures 5

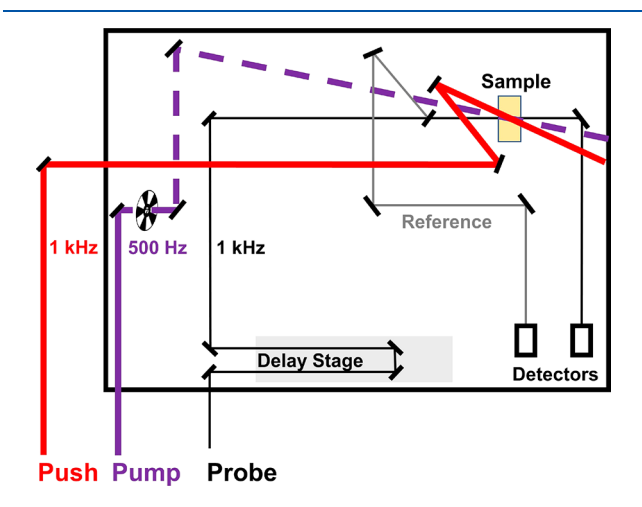


Figure 5. Schematic of pump-push-probe spectroscopy. The pump pulse (500 Hz) is first incident on the sample, followed by the push pulse (1 kHz) \sim 6 ps later. The probe pulse (1 kHz) is on an adjustable delay stage (-1.0 to 12 ps for these experiments).

and S6, respectively. We use this pump-push-probe spectroscopic technique to glean experimental information about the dynamics in higher-lying excited states that we postulated previously based on our computational results. Pump-push-probe spectroscopy has recently been utilized by a number of authors to monitor charge-separation dynamics in organic materials often used in solar cells. S1-58 Such results have demonstrated that photocurrent generation efficiency is governed by access to delocalized intermolecular charge-separated states. In the case of thin-film heterojunction organic solar cells, the role of the push pulse is to impart additional energy to overcome the activation barrier for accessing these delocalized charge-separated states.

In the context of photochemical reactivity, pump-pushprobe spectroscopy allows us to infer information concerning the potential role of the mixed $n\pi^*/\pi\pi^*$ excitations of the H- bonded complex in promoting access to the reactive CT state. In principle, the excited state prepared by the initial pump pulse (365 nm) could be further excited by the energy of the push pulse (1150 nm). However, these higher excited states are depopulated on femtosecond time scales by either nearly barrierless PCET or by efficient radiationless relaxation to the minimum of the S_1 state. The push pulse therefore interacts with the population in the long-lived S_1 reservoir state. As we mentioned previously, the photon energy of the push pulse was chosen, based upon the EADS in Figure 4a, to impart a nearly resonant perturbation to the H-bonded excited-state complex in the S_1 state at 6 ps after the pump pulse.

Using a third laser pulse (broadband probe), we monitor the sample's dynamic response to the pump and push pulses by recording time-dependent changes in transmission. Figure 6a shows the transient absorption spectra with and without the push pulse (both averaged from 6.5–8.0 ps) for TAHz in the presence of PhOH. The spectral evolution following the push pulse reveals a decrease in the excited-state signal amplitude associated with the S₁ state.

Interestingly, the impulsive decrease in $\Delta\Delta$ OD signal amplitude resulting from the push pulse in Figure 6a is persistent in the presence of PhOH on the time scale of our experiment. Parts b and c of Figure 6 show the signal probed from 700-750 nm and 900-1000 nm, respectively. This persistent loss in $\Delta\Delta$ OD amplitude suggests that the population of the S₁ reservoir state is propelled to a higherlying excited state, a portion of which, upon coupling to the CT electronic manifold, can relax by PCET toward the ·TAHzH/PhO· biradical state. In principle, the push pulse could be repeated after another few picoseconds, and more population of the S₁ reservoir state could be converted to BR products by PCET. This scheme allows us to control the branching ratio between reactive events (BR formation) and nonreactive events (S₁ luminescence) following the initial excitation of the TAHz:R-PhOH complex.

To verify that the system responds linearly to the power of the push, we performed a push-pulse power-dependence study, the results of which are shown in Figure S7. The effect of the push pulse is indeed linear with increasing power over the range of fluences used in this work. Therefore, the push pulse does not itself appear to be driving any two-photon processes under NIR excitation.

Figure 7a shows the transient absorption spectrum of TAHz in neat toluene overlaid with the spectra of TAHz in the presence of PhOH, Cl-PhOH, Me-PhOH, and MeO-PhOH with and without the push pulse (averaged from 6.5 to 8.0 ps). We observe static quenching of the TA signal with the addition

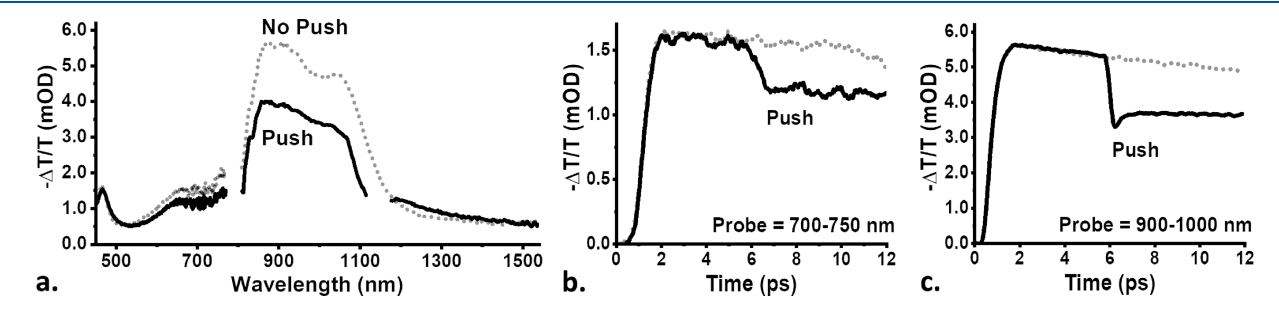


Figure 6. (a) Transient absorption spectra of TAHz ($50 \mu M$) in toluene and phenol (1.0 M) with the push pulse (solid lines) and without the push pulse (dotted lines) averaged from 6.5-8.0 ps. Temporal traces averaged over (b) 700-750 nm and (c) 900-1000 nm. The system was pumped at 365 nm and pushed at 1150 nm. The sample was stirring throughout the experiment.

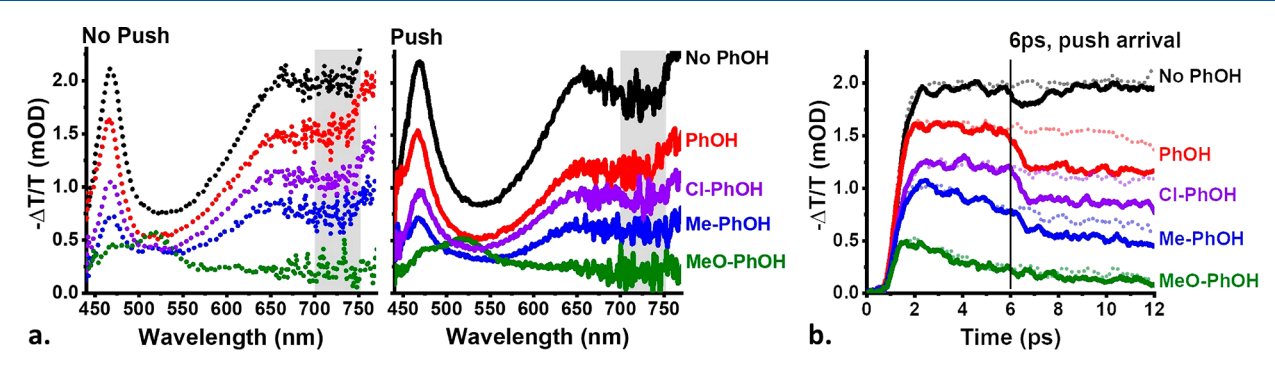


Figure 7. (a) (Left, dotted) Pump–probe spectra of TAHz ($50 \mu M$) in toluene with and without phenol derivatives, R-PhOH. (Right, solid) Pump-push-probe spectra of TAHz ($50 \mu M$) in toluene with and without phenol derivatives, R-PhOH. Spectra were averaged from 6.5–8.0 ps. (b) Decay of the population probed from 700–750 nm, shaded in gray in (a), with (solid) and without (dotted) the push pulse. The system was pumped at 365 nm and pushed at 1150 nm at 6 ps. The sample was continuously stirring during the experiment.

of each R-PhOH derivative, similar to previous luminescence experiments. The magnitude of this quenching increases with the electron-donating character of the substituent on R-PhOH. After the push pulse, many of the spectra exhibit a decrease in the signal amplitude, as demonstrated in Figure 6a. The change in spectral shape is least significant, almost nonexistent, for TAHz:MeO-PhOH, suggesting that in this case the excited-state population is not significantly altered by the push pulse. This is due to the highly reactive nature of the photoexcited TAHz:MeO-PhOH complex, producing radicals readily upon excitation from the pump without the assistance of the additional energy provided by the push pulse. The spectra in Figure 7a are overlaid in Figure S8 for closer comparison.

Figure 7b shows how the push pulse influences the dynamics in the 700–750 nm region of the TA spectrum on the picosecond time scale for the series of TAHz:R-PhOH complexes, in contrast to the excited-state push response of TAHz in neat toluene. Similar to Figure 6c, Figure 7b demonstrates persistent TA signal reduction, of varying degrees, of the excited state in the presence of R-PhOH, which suggests additional reactivity toward the ·TAHzH/R-PhO· biradical state, as discussed earlier.

The response we observe in Figure 7b for TAHz in neat toluene contrasts significantly with the results we observe for the TAHz:R-PhOH complexes. When PhOH is present, there is an irreversible loss of the transient absorption signal after the arrival of the push pulse. PhOH exhibits the largest signal loss (\sim 25%), while MeO-PhOH shows the smallest push-induced signal loss (<5%). However, without R-PhOH present (i.e., the "No PhOH" case), a small fraction of the S₁ population is pushed to the S_n states, which induces a transient loss of the absorption intensity in the 700–750 nm region. Yet this TA signal rapidly recovers, roughly within the duration of our push pulse (<200 fs), and the signal magnitude after 8 ps with the push pulse is virtually indistinguishable from that without the push pulse.

Further investigation shows the dynamic response to the push pulse in the 500–550 nm spectral regions with and without R-PhOH; see Figure S9. In this region, we observe an increase in the amplitude of the induced absorption signal that rapidly decays within the duration of the push pulse, which is consistent with internal conversion of the free TAHz chromophore from an upper excited state. These data support our hypothesis that the push pulse excites the hydrogen-bonded complex from the S₁ reservoir state into an upper excited state, and, depending on the presence and type of R-

PhOH, a fraction of the excited population couples to the CT state and, subsequently, yields radical products. In the case of MeO-PhOH, the push pulse does not significantly influence the amplitude of the TA signal, which suggests that, in the case of MeO-PhOH after the initial 365 nm excitation, the reaction dynamics already proceeds mainly along a trajectory toward the biradical products. These results appear to be consistent with prior predictions of barrierless excited-state reactivity in the TAHz:MeO-PhOH complex⁴³ and with the general trend predicted here in Table S2 derived from ab initio electronic-structure calculations.

We note that the shape of the resulting spectral signature that we obtain in the TA spectra for TAHz:MeO-PhOH complex is markedly dissimilar to the TA spectra for all other TAHz:R-PhOH complexes that we have measured in this study. In fact, the TA spectrum for the TAHz:MeO-PhOH system strongly resembles the induced absorption signal that we would associate with the reduced form of the TAHz chromophore. While the thermochemistry of this particular complex is such that both PCET and pure electron-transfer reactions may be accessible, we have previously measured the rate of fluorescence quenching using dimethoxybenzene, which possesses a similar oxidation potential as MeO-PhOH, and found it to be relatively sluggish compared to the quenching that we observe for MeO-PhOH. This result suggests that, while pure electron transfer can quench the TAHz excited state, it does not appear to account for the rapid reaction dynamics that we observe for MeO-PhOH. Additionally, the fact that we have detected photogeneration of spin-trapped phenoxyl radical DMPO adducts by EPR is a strong indication that the TAHz:MeO-PhOH complex undergoes a photondriven H atom abstraction reaction.

Finally, examination of the schematic potential energy landscape depicted in Figure 2 may lead one to conclude that, once the system relaxes to the low-lying S_1 reservoir state of the TAHz:PhOH system, no photochemical reaction will occur. While the potential energy barrier for the H atom transfer reaction is indeed significant in this case (calculated as 0.17 eV for TAHz:PhOH), ⁴³ we do observe luminescence quenching from this state in the presence of phenol on a time scale of nanoseconds. ⁴³ This observation is a clear indication that H atom transfer from PhOH to TAHz takes place even for H atom transfer barriers of several tenths of an electronvolt, owing to the absence of competing fast quenching processes in the S_1 state, such as intersystem crossing to triplet states (the S_1 state of TAHz is located 0.25 eV below the T_1 state). ⁵⁹

Further work is underway by our team to assess the possible roles that tunneling compared to thermal activation play in controlling the rate constants for these quenching processes.

CONCLUSIONS

Herein, we have demonstrated ultrafast photochemical control of excited-state intermolecular H atom abstraction reactions between the aza-aromatic TAHz model compound and various phenol derivatives. Although aza-aromatic photochemistry in protic solvents has been studied extensively since the mid-1900s, the underlying processes of coupled proton and electron transfer, specifically in heptazine-based systems, are not well-understood. Here we examined the coupled proton and electron motion in TAHz:R-PhOH hydrogen-bonded complexes and the correlation between ultrafast intermolecular charge transfer and the photochemical reactivity resulting in phenoxyl radicals. Furthermore, predictively controlling such reactions with color-tunable optical pulses is a longstanding goal in the field of photochemistry. Clarifying the connection between femtosecond to nanosecond dynamics and millisecond to minute chemical reactions has the potential to provide insight into materials design rules to manipulate photoinduced PCET reactions.

We demonstrated that altering the excited-state landscape of hydrogen-bonded TAHz-R-PhOH complexes by a substituent on R-PhOH can dramatically change the photochemical branching ratios after the initial excitation. Our data suggest that the fraction of excitations that underwent photoinduced PCET upon the initial 365 nm pulse was correlated with the increasing electron-donating strength of the substituent, R, on R-PhOH. In the TAHz:MeO-PhOH complex, for which the calculations predict a barrierless PCET reaction, the push pulse caused little to no change in the excited-state dynamics. This result suggests that the trajectory of this photochemical reaction is likely decided by the initial 365 nm excitation, at a rate that approaches the sub-ps time scale. For the Me-PhOH, PhOH, and Cl-PhOH complexation partners, on the other hand, the resonant excitation by the push pulse has a significant effect on the pump-induced excited-state population via the promotion of population from the relaxed S_1 reservoir state to the higher excited states of TAHz, which are quasidegenerate with the reactive CT state and drive the formation of the biradical product. The TAHz:R-PhOH complexes are fascinatingly simple systems in which the light-driven oxidation of solvent molecules (here, R-PhOH) can be controlled at will with appropriately tailored laser pulses.

Our time-resolved multipulse spectroscopy results supported by ab initio calculations provide synthetic chemists and materials scientists with new insight into photochemical reaction pathways that are germane to engineering new materials for solar fuel generation. Experimental efforts are underway in our lab to accelerate photoinduced PCET reactions without the need of additional energy from push pulses. To do this we are installing electron-withdrawing groups onto the heptazine core. It is predicted by theory that such substituents have a strong impact on the energy of the reactive CT state and therefore should mimic the effect of strong electron-donating substituents on PhOH demonstrated herein. This installation will shift the absorbing state of the hydrogen-bonded state closer to the reactive CT state, possibly allowing a barrierless transition, which would increase the efficiency of the photoinitiated one-electron oxidation of the solvent (preferably water).

ASSOCIATED CONTENT

Supporting Information

The Supporting Information is available free of charge at https://pubs.acs.org/doi/10.1021/acs.jpcc.0c00415.

Materials and methods, additional ultrafast spectroscopic discussion, and computational results (PDF)

AUTHOR INFORMATION

Corresponding Author

Cody W. Schlenker — Department of Chemistry, Molecular Engineering & Sciences Institute, and Clean Energy Institute, University of Washington, Seattle, Washington 98195, United States; Orcid.org/0000-0003-3103-402X; Email: schlenk@uw.edu

Authors

Kathryn L. Corp − Department of Chemistry, University of Washington, Seattle, Washington 98195, United States; orcid.org/0000-0002-2015-386X

Emily J. Rabe — Department of Chemistry, University of Washington, Seattle, Washington 98195, United States; orcid.org/0000-0002-9397-049X

Xiang Huang – Department of Chemistry, Technical University of Munich, D-85747 Garching, Germany

Johannes Ehrmaier – Department of Chemistry, Technical University of Munich, D-85747 Garching, Germany

Mitchell E. Kaiser – Department of Chemistry, University of Washington, Seattle, Washington 98195, United States

Andrzej L. Sobolewski — Institute of Physics, Polish Academy of Sciences, PL-02-668 Warsaw, Poland; ⊚ orcid.org/0000-0001-5718-489X

Wolfgang Domcke — Department of Chemistry, Technical University of Munich, D-85747 Garching, Germany; orcid.org/0000-0001-6523-1246

Complete contact information is available at: https://pubs.acs.org/10.1021/acs.jpcc.0c00415

Note:

The authors declare no competing financial interest.

ACKNOWLEDGMENTS

This work is based on research that was supported in part by the Washington Research Foundation and the University of Washington Clean Energy Institute. C.W.S. acknowledges that a portion of this material is based upon work supported by the U.S. National Science Foundation (NSF) under Grant no. CHE-1846480. We are extremely grateful for the assistance of the Stoll lab at the University of Washington during the EPR training, data collection, and data analysis. A portion of this work was conducted at the Molecular Analysis Facility, a National Nanotechnology Coordinated Infrastructure site at the University of Washington, which is supported in part by the National Science Foundation (Grant ECC-1542101), Office of Naval Research Defense University Research Instrumentation Program (Grant no. 0014-14-1-0757), University of Washington, Molecular Engineering & Sciences Institute, Clean Energy Institute, and National Institutes of Health. The work at the Technical University of Munich (J.E. and W.D.) was supported by the Deutsche Forschungsgemeinschaft (DFG) through the Munich Centre for Advanced Photonics (MAP) and by the Max Planck Society through the International Max Planck Research School of Advanced

Photon Science (IMPRS-APS). A.L.S. acknowledges support by the Alexander von Humboldt Research Award.

REFERENCES

- (1) Wang, S.; Wang, X. Imidazolium Ionic Liquids, Imidazolylidene Heterocyclic Carbenes, and Zeolitic Imidazolate Frameworks for CO_2 Capture and Photochemical Reduction. *Angew. Chem., Int. Ed.* **2016**, 55 (7), 2308–2320.
- (2) Kumar, S.; Kumar, A.; Bahuguna, A.; Sharma, V.; Krishnan, V. Two-Dimensional Carbon-Based Nanocomposites for Photocatalytic Energy Generation and Environmental Remediation Applications. *Beilstein J. Nanotechnol.* **2017**, *8*, 1571–1600.
- (3) Ong, W.-J.; Tan, L.-L.; Ng, Y. H.; Yong, S.-T.; Chai, S.-P. Graphitic Carbon Nitride (g- C_3N_4)-Based Photocatalysts for Artificial Photosynthesis and Environmental Remediation: Are We a Step Closer To Achieving Sustainability? *Chem. Rev.* **2016**, *116* (12), 7159–7329.
- (4) Roy, S.; Ardo, S.; Furche, F. 5-Methoxyquinoline Photobasicity Is Mediated by Water Oxidation. *J. Phys. Chem. A* **2019**, *123* (31), 6645–6651.
- (5) Hunt, J. R.; Dawlaty, J. M. Photodriven Deprotonation of Alcohols by a Quinoline Photobase. *J. Phys. Chem. A* **2018**, *122* (40), 7931–7940.
- (6) Wasielewski, M. R. Photoinduced Electron Transfer in Supramolecular Systems for Artificial Photosynthesis. *Chem. Rev.* **1992**, 92 (3), 435–461.
- (7) Stermitz, F. R.; Wei, C. C.; O'Donnell, C. M. Photochemistry of N-Heterocycles. V. Photochemistry of Quinoline and Some Substituted Quinoline Derivatives. *J. Am. Chem. Soc.* **1970**, 92 (9), 2745–2752.
- (8) Stermitz, F. R.; Wei, C. C. Photochemistry of Aromatic N-Heterocycles. IV. McLafferty Rearrangement and Type II Photocleavage Comparisons in a New System. 2-Substituted Quinolines. *J. Am. Chem. Soc.* **1969**, *91* (11), 3103–3104.
- (9) Chapman, O. L. Organic Photochemistry, Vol. 2; Dekker: 1969.
- (10) Connolly, J. S.; Linschitz, H. Photoaddition of Alcohols to Purine. *Photochem. Photobiol.* **1968**, 7 (6), 791–806.
- (11) Whitten, D. G.; Lee, Y. J. Reactions of Hidden n, π^* Excited States in N-Heteroaromatics. Photoreduction and Photoaddition. *J. Am. Chem. Soc.* **1970**, 92 (2), 415–416.
- (12) Herkstroeter, W. G.; Hammond, G. S. Mechanisms of Photochemical Reactions in Solution. XXXIX. Study of Energy Transfer by Kinetic Spectrophotometry. *J. Am. Chem. Soc.* **1966**, 88 (21), 4769–4777.
- (13) Weinberg, D. R.; Gagliardi, C. J.; Hull, J. F.; Murphy, C. F.; Kent, C. A.; Westlake, B. C.; Paul, A.; Ess, D. H.; McCafferty, D. G.; Meyer, T. J. Proton-Coupled Electron Transfer. *Chem. Rev.* **2012**, *112* (7), 4016–4093.
- (14) Gagliardi, C. J.; Westlake, B. C.; Kent, C. A.; Paul, J. J.; Papanikolas, J. M.; Meyer, T. J. Integrating Proton Coupled Electron Transfer (PCET) and Excited States. *Coord. Chem. Rev.* **2010**, 254 (21), 2459–2471.
- (15) Whitten, D. G.; Lee, Y. J. Photochemistry of Aza Aromatics. Identification of the Reactive Intermediate in the Photoreduction of Acridine. *J. Am. Chem. Soc.* **1971**, *93* (4), *961*–*966*.
- (16) Kellmann, A.; Dubois, J. T. Photoreactive State of Acridine in Solution. J. Chem. Phys. 1965, 42 (7), 2518–2522.
- (17) Kikuchi, K.; Kasama, K.; Kanemoto, A.; Ujiie, K.; Kikubun, H. Reaction and Deactivation of Excited Acridine in Ethanol. *J. Phys. Chem.* **1985**, 89 (5), 868–871.
- (18) Donckt, E. V.; Porter, G. Role of the $3(n-\pi^*)$ State in the Photoreduction of Acridine. *J. Chem. Phys.* **1967**, 46 (3), 1173–1175.
- (19) Wilkinson, F.; Dubois, J. T. Reactive State in the Photoreduction of Acridine in Ethanol. *J. Chem. Phys.* **1968**, 48 (6), 2651–2654
- (20) Koizumi, M.; Ikeda, Y.; Iwaoka, T. Reactive State of Acridine in the Photoreduction in Alcohols. *J. Chem. Phys.* **1968**, 48 (4), 1869–1870.

- (21) Eisenhart, T. T.; Dempsey, J. L. Photo-induced Proton-Coupled Electron Transfer Reactions of Acridine Orange: Comprehensive Spectral and Kinetics Analysis. *J. Am. Chem. Soc.* **2014**, *136* (35), 12221–12224.
- (22) Liu, X.; Karsili, T. N. V.; Sobolewski, A. L.; Domcke, W. Photocatalytic Water Splitting with the Acridine Chromophore: A Computational Study. *J. Phys. Chem. B* **2015**, *119* (33), 10664–10672.
- (23) Ehrmaier, J.; Karsili, T. N. V.; Sobolewski, A. L.; Domcke, W. Mechanism of Photocatalytic Water Splitting with Graphitic Carbon Nitride: Photochemistry of the Heptazine-Water Complex. *J. Phys. Chem. A* **2017**, *121* (25), 4754–4764.
- (24) Ehrmaier, J.; Janicki, M. J.; Sobolewski, A. L.; Domcke, W. Mechanism of Photocatalytic Water Splitting with Triazine-Based Carbon Nitrides: Insights From Ab Initio Calculations for the Triazine-Water Complex. *Phys. Chem. Chem. Phys.* **2018**, 20 (21), 14420–14430.
- (25) Liu, J.; Liu, Y.; Liu, N.; Han, Y.; Zhang, X.; Huang, H.; Lifshitz, Y.; Lee, S. T.; Zhong, J.; Kang, Z. Water Splitting. Metal-Free Efficient Photocatalyst for Stable Visible Water Splitting via a Two-Electron Pathway. *Science* **2015**, 347 (6225), 970–4.
- (26) Moniz, S. J. A.; Shevlin, S. A.; Martin, D. J.; Guo, Z. X.; Tang, J. W. Visible-Light Driven Heterojunction Photocatalysts for Water Splitting A Critical Review. *Energy Environ. Sci.* **2015**, 8 (3), 731–759.
- (27) Rahman, M. Z.; Davey, K.; Qiao, S.-Z. Carbon, Nitrogen and Phosphorus Containing Metal-Free Photocatalysts for Hydrogen Production: Progress and Challenges. *J. Mater. Chem. A* **2018**, *6* (4), 1305–1322.
- (28) Wen, J. Q.; Xie, J.; Chen, X. B.; Li, X. A Review on g- C_3N_4 -Based Photocatalysts. *Appl. Surf. Sci.* **2017**, 391, 72–123.
- (29) Ye, S.; Wang, R.; Wu, M. Z.; Yuan, Y. P. A Review on g-C₃N₄ for Photocatalytic Water Splitting and CO₂ Reduction. *Appl. Surf. Sci.* **2015**, 358, 15–27.
- (30) Zhu, B.; Zhang, L.; Cheng, B.; Yu, J. First-Principle Calculation Study of Tri-s-triazine-Based g- C_3N_4 : A Review. *Appl. Catal., B* **2018**, 224, 983–999.
- (31) Liu, X.; Dai, L. Carbon-Based Metal-Free Catalysts. Nat. Rev. Mater. 2016, 1, 16064.
- (32) Wang, X.; Maeda, K.; Thomas, A.; Takanabe, K.; Xin, G.; Carlsson, J. M.; Domen, K.; Antonietti, M. A Metal-Free Polymeric Photocatalyst for Hydrogen Production from Water under Visible Light. *Nat. Mater.* **2009**, *8*, 76–80.
- (33) Liu, J. H.; Zhang, T. K.; Wang, Z. C.; Dawson, G.; Chen, W. Simple Pyrolysis of Urea into Graphitic Carbon Nitride with Recyclable Adsorption and Photocatalytic Activity. *J. Mater. Chem.* **2011**, *21* (38), 14398–14401.
- (34) Lau, V. W. H.; Yu, V. W. Z.; Ehrat, F.; Botari, T.; Moudrakovski, I.; Simon, T.; Duppel, V.; Medina, E.; Stolarczyk, J. K.; Feldmann, J.; et al. Urea-Modified Carbon Nitrides: Enhancing Photocatalytic Hydrogen Evolution by Rational Defect Engineering. *Adv. Energy Mater.* 2017, 7 (12), 1602251.
- (35) Liu, J.; Zhang, Y.; Lu, L.; Wu, G.; Chen, W. Self-Regenerated Solar-Driven Photocatalytic Water-Splitting by Urea Derived Graphitic Carbon Nitride with Platinum Nanoparticles. *Chem. Commun.* **2012**, *48* (70), 8826–8838.
- (36) Kharlamov, A.; Bondarenko, M.; Kharlamova, G.; Gubareni, N. Features of the Synthesis of Carbon Nitride Oxide (g-C₃N₄)O at Urea Pyrolysis. *Diamond Relat. Mater.* **2016**, *66*, 16–22.
- (37) Shi, L.; Liang, L.; Wang, F. X.; Liu, M. S.; Chen, K. L.; Sun, K. N.; Zhang, N. Q.; Sun, J. M. Higher Yield Urea-Derived Polymeric Graphitic Carbon Nitride with Mesoporous Structure and Superior Visible-Light-Responsive Activity. ACS Sustainable Chem. Eng. 2015, 3 (12), 3412–3419.
- (38) Rabe, E. J.; Corp, K. L.; Sobolewski, A. L.; Domcke, W.; Schlenker, C. W. Proton-Coupled Electron Transfer from Water to a Model Heptazine-Based Molecular Photocatalyst. *J. Phys. Chem. Lett.* **2018**, 9 (21), 6257–6261.

- (39) Zhang, J.; Zhang, G.; Chen, X.; Lin, S.; Mohlmann, L.; Dolega, G.; Lipner, G.; Antonietti, M.; Blechert, S.; Wang, X. Co-Monomer Control of Carbon Nitride Semiconductors to Optimize Hydrogen Evolution with Visible Light. *Angew. Chem., Int. Ed.* **2012**, *51* (13), 3183–7.
- (40) Schroder, M.; Kailasam, K.; Borgmeyer, J.; Neumann, M.; Thomas, A.; Schomacker, R.; Schwarze, M. Hydrogen Evolution Reaction in a Large-Scale Reactor using a Carbon Nitride Photocatalyst under Natural Sunlight Irradiation. *Energy Technol.* **2015**, 3 (10), 1014–1017.
- (41) Corp, K. L.; Schlenker, C. W. Ultrafast Spectroscopy Reveals Electron-Transfer Cascade That Improves Hydrogen Evolution with Carbon Nitride Photocatalysts. *J. Am. Chem. Soc.* **2017**, *139* (23), 7904–7912.
- (42) Domcke, W.; Ehrmaier, J.; Sobolewski, A. L. Solar Energy Harvesting with Carbon Nitrides and N-Heterocyclic Frameworks: Do We Understand the Mechanism? *Chem. Photo. Chem.* **2019**, 3 (1), 10–23.
- (43) Rabe, E. J.; Corp, K. L.; Huang, X.; Ehrmaier, J.; Flores, R. G.; Estes, S. L.; Sobolewski, A. L.; Domcke, W.; Schlenker, C. W. Barrierless Heptazine-Driven Excited-State Proton-Coupled Electron Transfer: Implications for Controlling Photochemistry of Carbon Nitrides and Aza-Arenes. *J. Phys. Chem. C* **2019**, *123*, 29580–29588. (44) Ullah, N.; Chen, S.; Zhao, Y.; Zhang, R. Photoinduced Water–Heptazine Electron-Driven Proton Transfer: Perspective for Water
- Splitting with g-C3N4. *J. Phys. Chem. Lett.* **2019**, *10*, 4310–4316. (45) Yamaji, M.; Oshima, J.; Hidaka, M. Verification of the Electron/Proton Coupled Mechanism for Phenolic H-Atom Transfer Using a Triplet π,π^* Carbonyl. *Chem. Phys. Lett.* **2009**, 475 (4–6), 235–239
- (46) Osako, T.; Ohkubo, K.; Taki, M.; Tachi, Y.; Fukuzumi, S.; Itoh, S. Oxidation Mechanism of Phenols by Dicopper–Dioxygen (Cu₂/O₂) Complexes. *J. Am. Chem. Soc.* **2003**, *125* (36), 11027–11033.
- (47) Bronner, C.; Wenger, O. S. Kinetic Isotope Effects in Reductive Excited-State Quenching of Ru(2,2'-Bipyrazine)₃²⁺ by Phenols. *J. Phys. Chem. Lett.* **2012**, 3 (1), 70–74.
- (48) Warren, J. J.; Tronic, T. A.; Mayer, J. M. Thermochemistry of Proton-Coupled Electron Transfer Reagents and its Implications. *Chem. Rev.* **2010**, *110* (12), 6961–7001.
- (49) Schirmer, J. Beyond the Random-Phase Approximation: A New Approximation Scheme for the Polarization Propagator. *Phys. Rev. A: At., Mol., Opt. Phys.* **1982**, 26 (5), 2395–2416.
- (50) Pinteala, M.; Schlick, S. Direct ESR Detection and Spin Trapping of Radicals Generated by Reaction of Oxygen Radicals with Sulfonated Poly(Ether Ether Ketone) (SPEEK) Membranes. *Polym. Degrad. Stab.* **2009**, 94 (10), 1779–1787.
- (51) Bakulin, A. A.; Rao, A.; Pavelyev, V. G.; van Loosdrecht, P. H. M.; Pshenichnikov, M. S.; Niedzialek, D.; Cornil, J.; Beljonne, D.; Friend, R. H. The Role of Driving Energy and Delocalized States for Charge Separation in Organic Semiconductors. *Science* **2012**, 335 (6074), 1340–1344.
- (52) Bakulin, A. A.; Silva, C.; Vella, E. Ultrafast Spectroscopy with Photocurrent Detection: Watching Excitonic Optoelectronic Systems at Work. *J. Phys. Chem. Lett.* **2016**, *7* (2), 250–258.
- (53) Dimitrov, S. D.; Bakulin, A. A.; Nielsen, C. B.; Schroeder, B. C.; Du, J.; Bronstein, H.; McCulloch, I.; Friend, R. H.; Durrant, J. R. On the Energetic Dependence of Charge Separation in Low-Band-Gap Polymer/Fullerene Blends. J. Am. Chem. Soc. 2012, 134 (44), 18189–18102
- (54) Mangold, H.; Bakulin, A. A.; Howard, I. A.; Kästner, C.; Egbe, D. A. M.; Hoppe, H.; Laquai, F. Control of Charge Generation and Recombination in Ternary Polymer/Polymer:Fullerene Photovoltaic Blends Using Amorphous and Semi-Crystalline Copolymers as Donors. *Phys. Chem. Chem. Phys.* **2014**, *16* (38), 20329–20337.
- (55) Tan, Z. K.; Johnson, K.; Vaynzof, Y.; Bakulin, A. A.; Chua, L. L.; Ho, P. K.; Friend, R. H. Suppressing Recombination in Polymer Photovoltaic Devices via Energy-Level Cascades. *Adv. Mater.* **2013**, 25 (30), 4131–8.

- (56) Zhang, J.; Jakowetz, A. C.; Li, G.; Di, D.; Menke, S. M.; Rao, A.; Friend, R. H.; Bakulin, A. A. On the Energetics of Bound Charge-Transfer States in Organic Photovoltaics. *J. Mater. Chem. A* **2017**, *S* (23), 11949–11959.
- (57) Cabanillas-Gonzalez, J.; Grancini, G.; Lanzani, G. Pump-Probe Spectroscopy in Organic Semiconductors: Monitoring Fundamental Processes of Relevance in Optoelectronics. *Adv. Mater.* **2011**, 23 (46), 5468–5485.
- (58) Paternò, G. M.; Moretti, L.; Barker, A. J.; Chen, Q.; Müllen, K.; Narita, A.; Cerullo, G.; Scotognella, F.; Lanzani, G. Pump-Push-Probe for Ultrafast All-Optical Switching: The Case of a Nanographene Molecule. *Adv. Funct. Mater.* **2019**, 29 (21), 1805249.
- (59) Ehrmaier, J.; Rabe, E. J.; Pristash, S. R.; Corp, K. L.; Schlenker, C. W.; Sobolewski, A. L.; Domcke, W. Singlet-Triplet Inversion in Heptazine and in Polymeric Carbon Nitrides. *J. Phys. Chem. A* **2019**, 123 (38), 8099–8108.